Numerical and Statistical Validation of a BCS-based Technique for Microwave Imaging under the Rytov Approximation

L. Poli, G. Oliveri, P. Rocca, A. Massa

Abstract

In this report, a statistical analysis of the BCS-based inversion technique for microwave imaging within the Rytov approximation is proposed. The performance of the technque has been evaluated varying the number and the position of the sparse objects inside the investiation domain. Moreover, a comparison with a state-of-the-art technique based on the Born approximation has been proposed.

Contents

1 Numerical Validation within Weak Sparsity Conditions of the Scatterers

1.1 TEST CASE: Statistical Test - Varying the number of the Scatterers

Goal: evaluate the performances of BCS

- Number of Views: V
- Number of Measurements: M
- Number of Cells for the Inversion: N
- Number of Cells for the Direct solver: D
- Side of the investigation domain: L

Test Case Description

Direct solver:

- Square domain divided in $\sqrt{D} \times \sqrt{D}$ cells
- Domain side: $L = 3\lambda$
- $D = 1296$ (discretization for the direct solver: $< \lambda/10$)

Investigation domain:

- Square domain divided in $\sqrt{N} \times \sqrt{N}$ cells
- $L = 3\lambda$
- $N = 324$

Measurement domain:

- Measurement points taken on a circle of radius $\rho = 3\lambda$
- Full-aspect measurements
- $M \approx 2ka \rightarrow M = 27$

Sources:

- Plane waves
- $V \approx 2ka \rightarrow V = 27$
- Amplitude $A = 1$
- Frequency: 300 MHz ($\lambda = 1$)

Object:

- S square cylinders of side $\frac{\lambda}{6} = 0.16667$ ($S \in \{1, 2, 3, 4, 5, 6\}$)
- $\varepsilon_r \in \{1.5, 2.0, 2.5, 3.0\}$
- $\sigma = 0$ [S/m]

BCS parameters:

- Initial estimate of the noise: $n_0 = 8.0 \times 10^{-3}$
- Convergenze parameter: $\tau = 1.0 \times 10^{-8}$

Statistical Analysis:

- $K = 10$ random seeds used for each case to determine the position of the objects inside the onvestigation domain

RESULTS: $\varepsilon_r = 1.5$

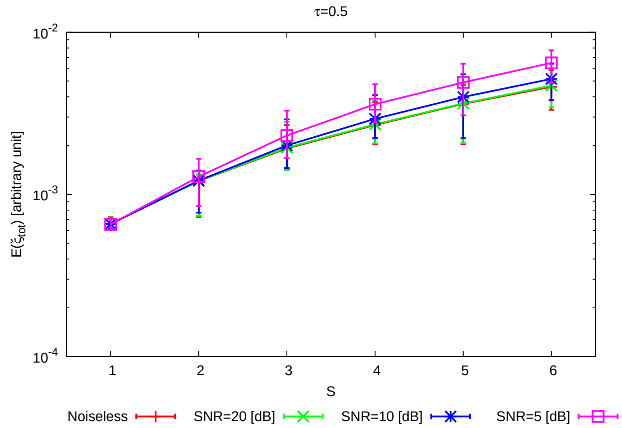

(a)

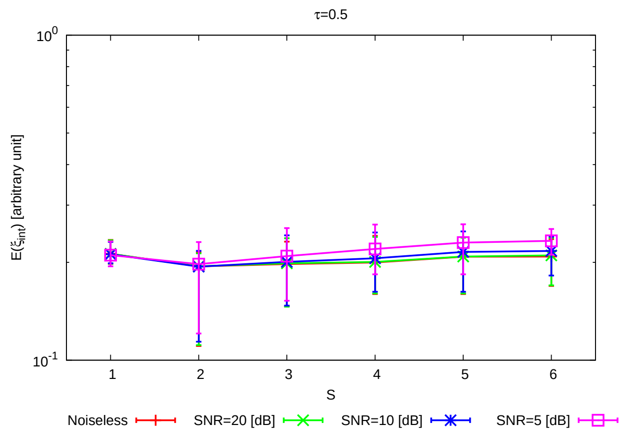

(b)

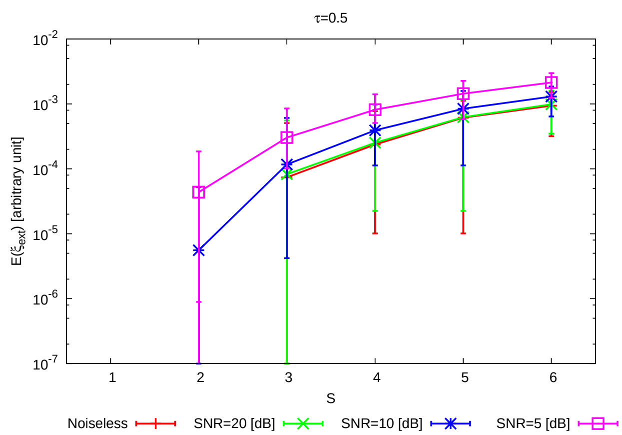

(c)

Figure 1. *Statistical analysis* $[K = 10,\ \varepsilon_r = 1.5]$ - Behaviour of mean, maximum and minimum of the error figures as a function of S (sparsity factor), for different SNR values: (a) total error ξ_{tot}, (b) internal error ξ_{int}, (c) external error ξ_{ext}.

RESULTS: $\varepsilon_r = 2.0$

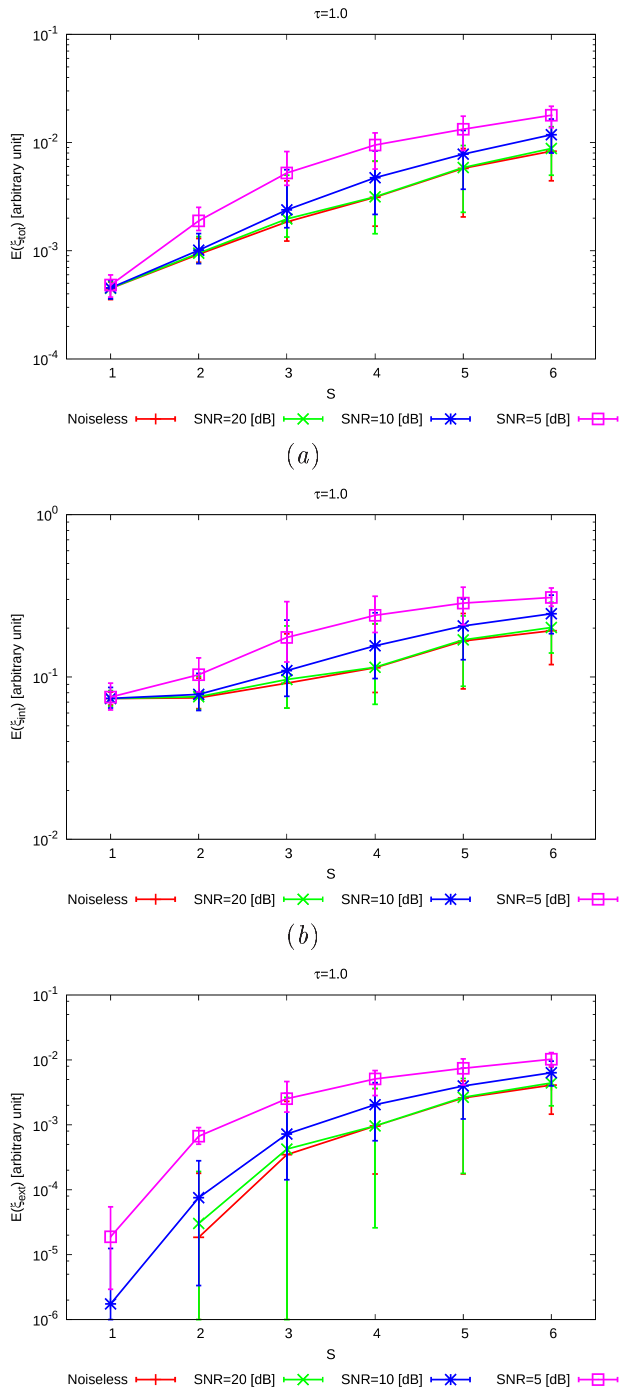

(c)

Figure 2. *Statistical analysis* $[K = 10,\ \varepsilon_r = 2.0]$ - Behaviour of mean, maximum and minimum of the error figures as a function of S (sparsity factor), for different SNR values: (a) total error ξ_{tot}, (b) internal error ξ_{int}, (c) external error ξ_{ext}.

RESULTS: $\varepsilon_r = 2.5$

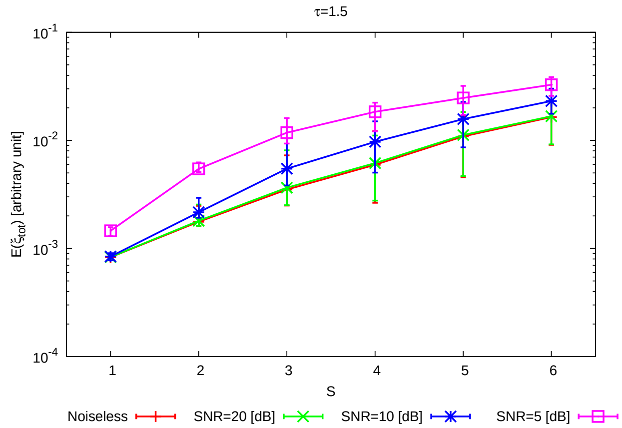

(a)

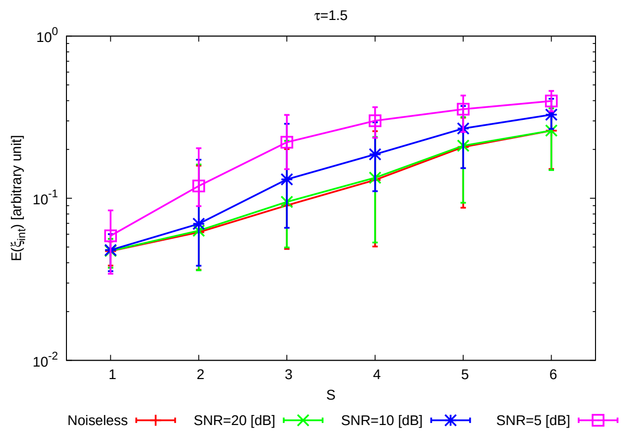

(b)

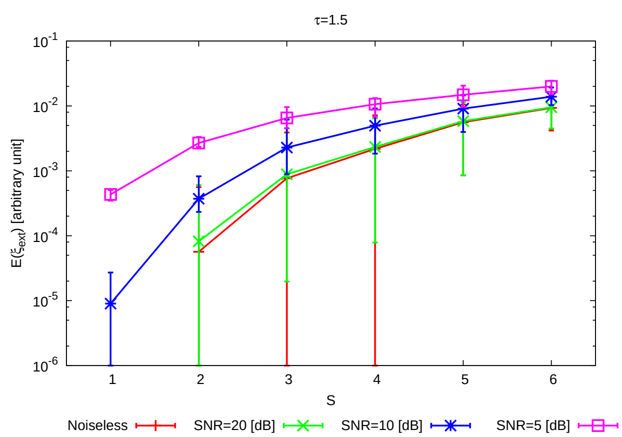

(c)

Figure 3. *Statistical analysis* $[K = 10, \varepsilon_r = 2.5]$ - Behaviour of mean, maximum and minimum of the error figures as a function of S (sparsity factor), for different SNR values: (a) total error ξ_{tot}, (b) internal error ξ_{int}, (c) external error ξ_{ext}.

RESULTS: $\varepsilon_r = 3.0$

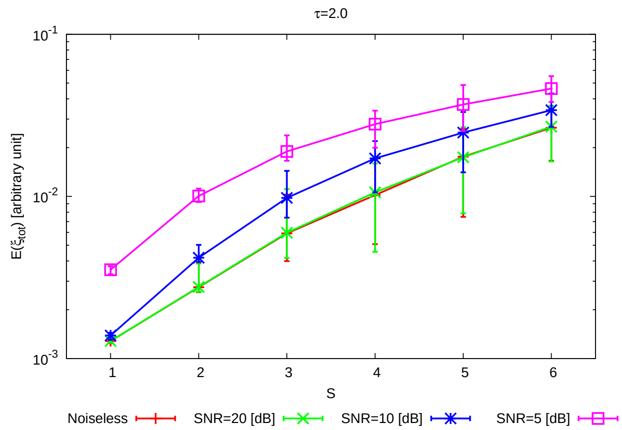

(a)

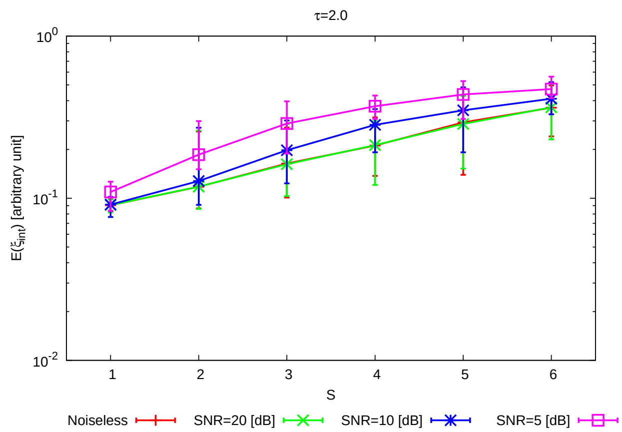

(b)

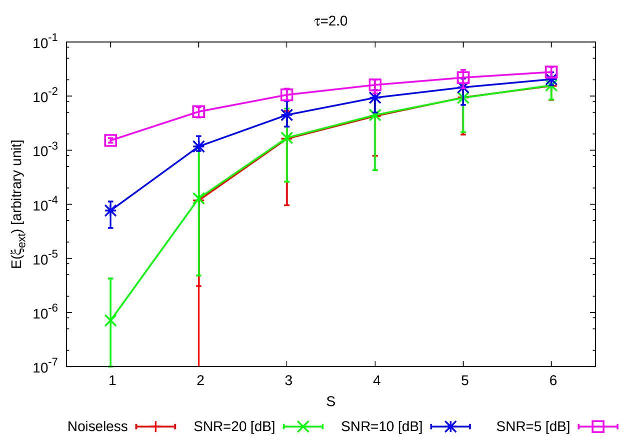

(c)

Figure 4. *Statistical analysis* $[K = 10, \varepsilon_r = 3.0]$ - Behaviour of mean, maximum and minimum of the error figures as a function of S (sparsity factor), for different SNR values: (a) total error ξ_{tot}, (b) internal error ξ_{int}, (c) external error ξ_{ext}.

1.2 TEST CASE: Variable Square Cylinder Dimension

Goal: evaluate the performances of BCS

- Number of Views: V
- Number of Measurements: M
- Number of Cells for the Inversion: N
- Number of Cells for the Direct solver: D
- Side of the investigation domain: L

Test Case Description

Direct solver:

- Square domain divided in $\sqrt{D} \times \sqrt{D}$ cells
- Domain side: $L = 3\lambda$
- $D = 1296$ (discretization for the direct solver: $< \lambda/10$)

Investigation domain:

- Square domain divided in $\sqrt{N} \times \sqrt{N}$ cells
- $L = 3\lambda$
- $N = 324$

Measurement domain:

- Measurement points taken on a circle of radius $\rho = 3\lambda$
- Full-aspect measurements
- $M \approx 2ka \rightarrow M = 27$

Sources:

- Plane waves
- $V \approx 2ka \rightarrow V = 27$
- Amplitude $A = 1$
- Frequency: 300 MHz ($\lambda = 1$)

Object:

- Square cylinder of side $L = \left\{\frac{\lambda}{6}, \frac{\lambda}{3}, \frac{\lambda}{2}, \frac{2}{3}\lambda, \frac{5}{6}\lambda, \lambda\right\}$
- $\varepsilon_r \in \{1.1, 1.2, 1.3, 1.4, 1.5, 2.0, 2.5, 3.0\}$
- $\sigma = 0$ [S/m]

BCS parameters:

- Initial estimate of the noise: $n_0 = 8.0 \times 10^{-3}$
- Convergenze parameter: $\tau = 1.0 \times 10^{-8}$

RESULTS: Variable Square Cylinder Dimension - $L = \frac{\lambda}{3}$ **-** $SNR = Noiseless$

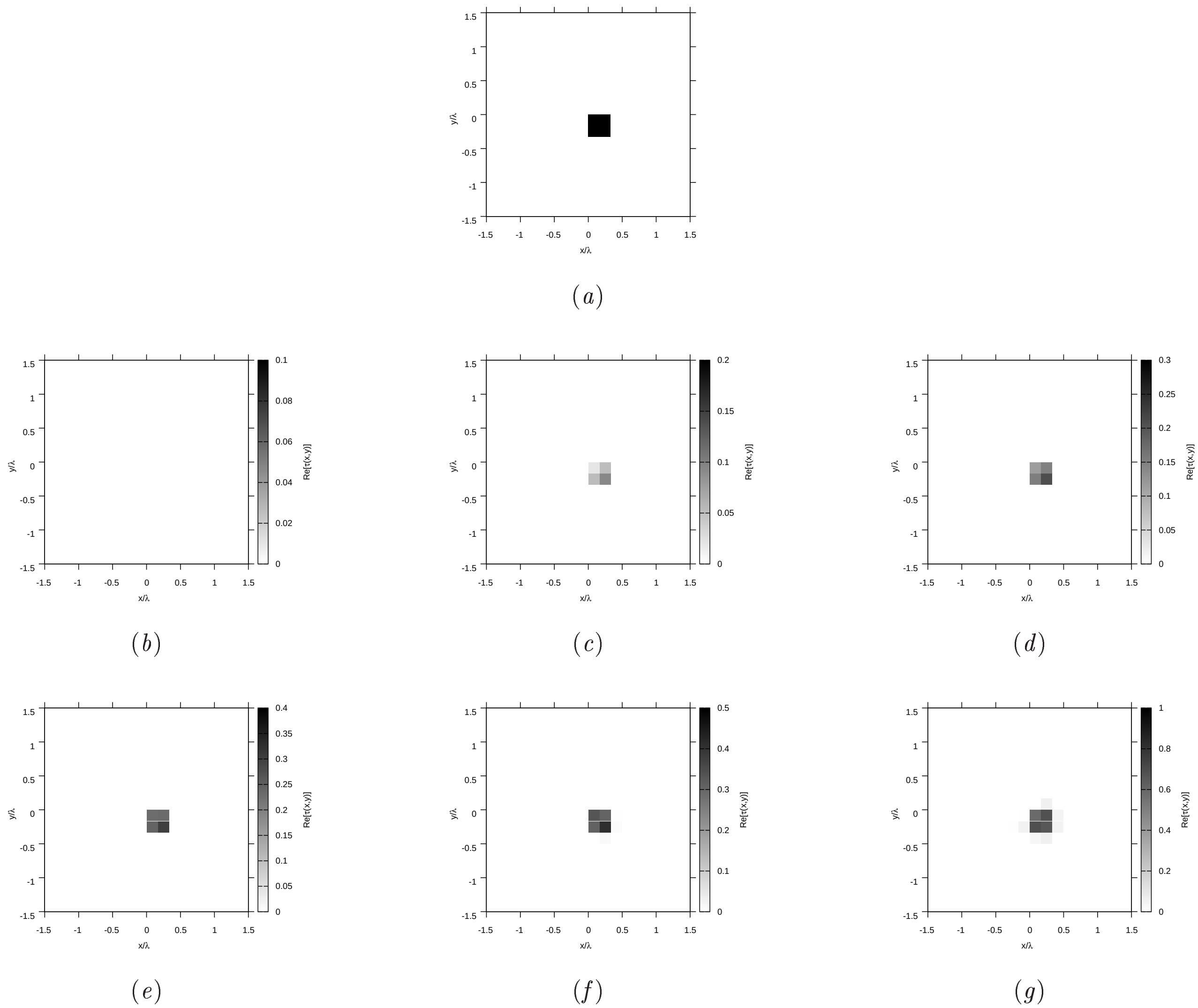

Figure 5. Actual object (a) and $(b)(c)(d)(e)(f)(g)$ BCS reconstructed object with (b) $\varepsilon_r = 1.1$, (c) $\varepsilon_r = 1.2$, (d) $\varepsilon_r = 1.3$, (e) $\varepsilon_r = 1.4$, (f) $\varepsilon_r = 1.5$ and (g) $\varepsilon_r = 2.0$.

RESULTS: Variable Square Cylinder Dimension - $L = \frac{\lambda}{3}$ **-** $SNR = 10\,[dB]$

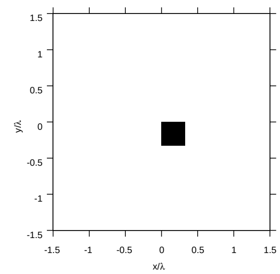

(a)

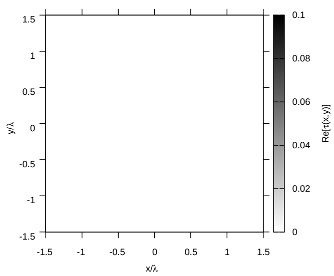

(b)

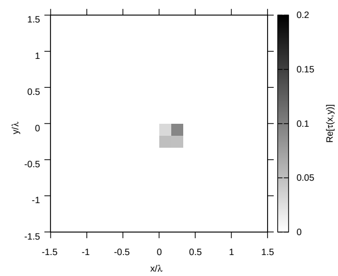

(c)

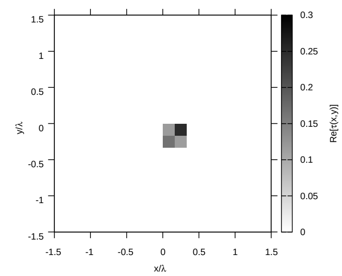

(d)

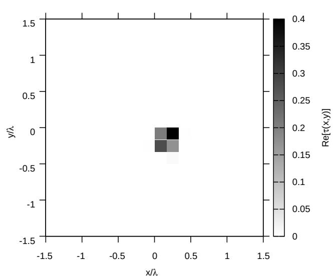

(e)

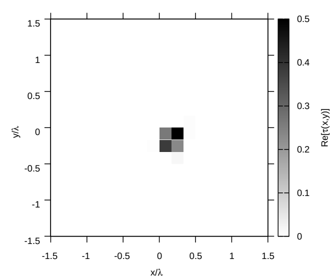

(f)

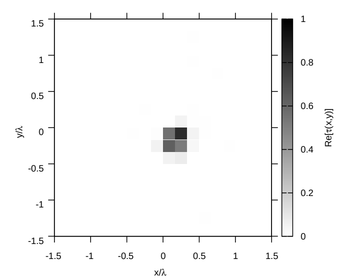

(g)

Figure 6. Actual object (a) and $(b)(c)(d)(e)(f)(g)$ BCS reconstructed object with (b) $\varepsilon_r = 1.1$, (c) $\varepsilon_r = 1.2$, (d) $\varepsilon_r = 1.3$, (e) $\varepsilon_r = 1.4$, (f) $\varepsilon_r = 1.5$ and (g) $\varepsilon_r = 2.0$.

RESULTS: Variable Square Cylinder Dimension - $L = \frac{\lambda}{3}$ **-** $SNR = 5\,[dB]$

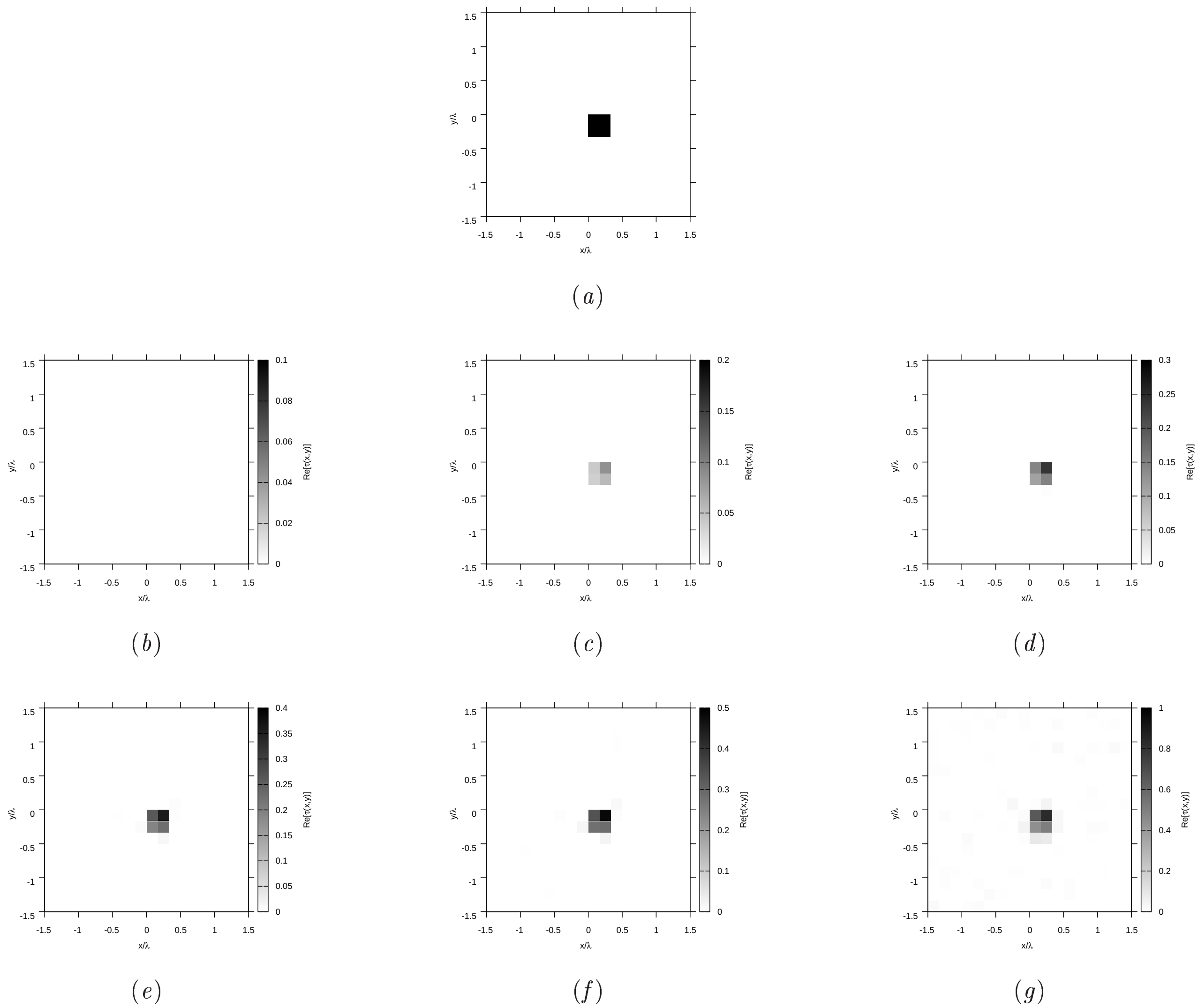

(a) (b) (c) (d) (e) (f) (g)

Figure 7. Actual object (a) and $(b)(c)(d)(e)(f)(g)$ BCS reconstructed object with (b) $\varepsilon_r = 1.1$, (c) $\varepsilon_r = 1.2$, (d) $\varepsilon_r = 1.3$, (e) $\varepsilon_r = 1.4$, (f) $\varepsilon_r = 1.5$ and (g) $\varepsilon_r = 2.0$.

RESULTS: Variable Square Cylinder Dimension - $L = \frac{\lambda}{3}$ **-** $SNR = Noiseless$

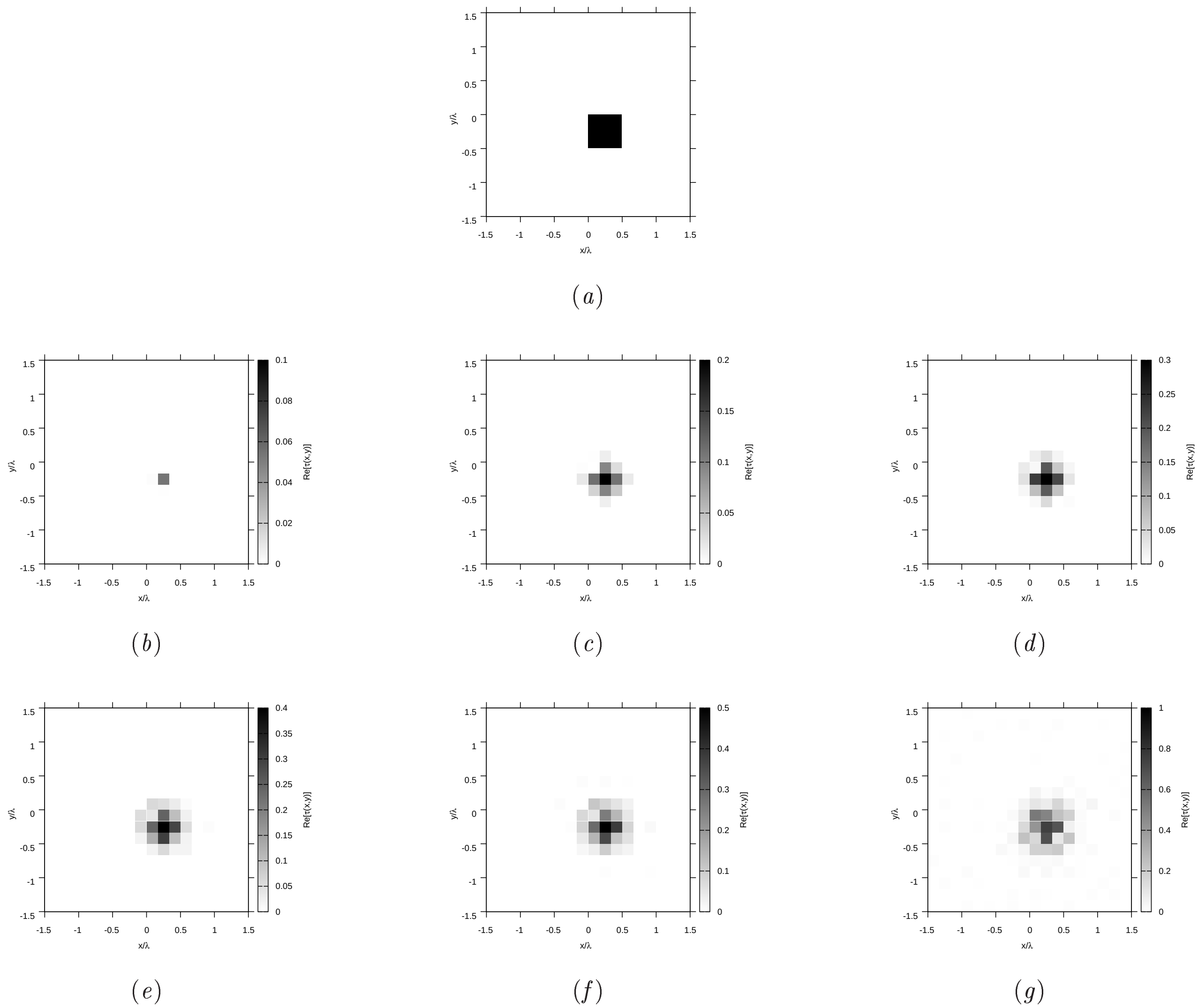

Figure 8. Actual object (a) and $(b)(c)(d)(e)(f)(g)$ BCS reconstructed object with (b) $\varepsilon_r = 1.1$, (c) $\varepsilon_r = 1.2$, (d) $\varepsilon_r = 1.3$, (e) $\varepsilon_r = 1.4$, (f) $\varepsilon_r = 1.5$ and (g) $\varepsilon_r = 2.0$.

RESULTS: Variable Square Cylinder Dimension - $L = \frac{\lambda}{3}$ **-** $SNR = 10\,[dB]$

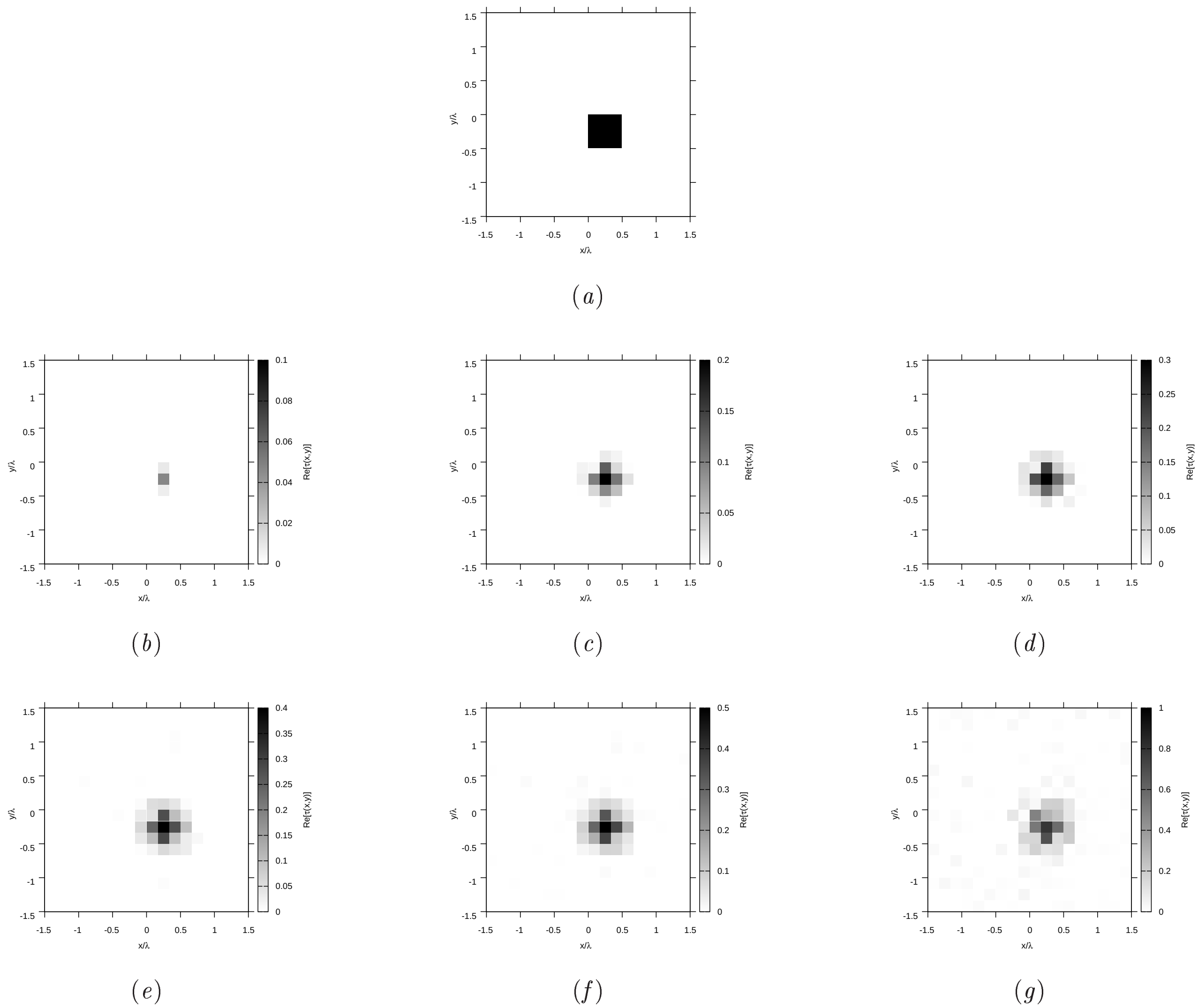

Figure 9. Actual object (a) and $(b)(c)(d)(e)(f)(g)$ BCS reconstructed object with (b) $\varepsilon_r = 1.1$, (c) $\varepsilon_r = 1.2$, (d) $\varepsilon_r = 1.3$, (e) $\varepsilon_r = 1.4$, (f) $\varepsilon_r = 1.5$ and (g) $\varepsilon_r = 2.0$.

RESULTS: Variable Square Cylinder Dimension - $L = \frac{\lambda}{3}$ **-** $SNR = 5\,[dB]$

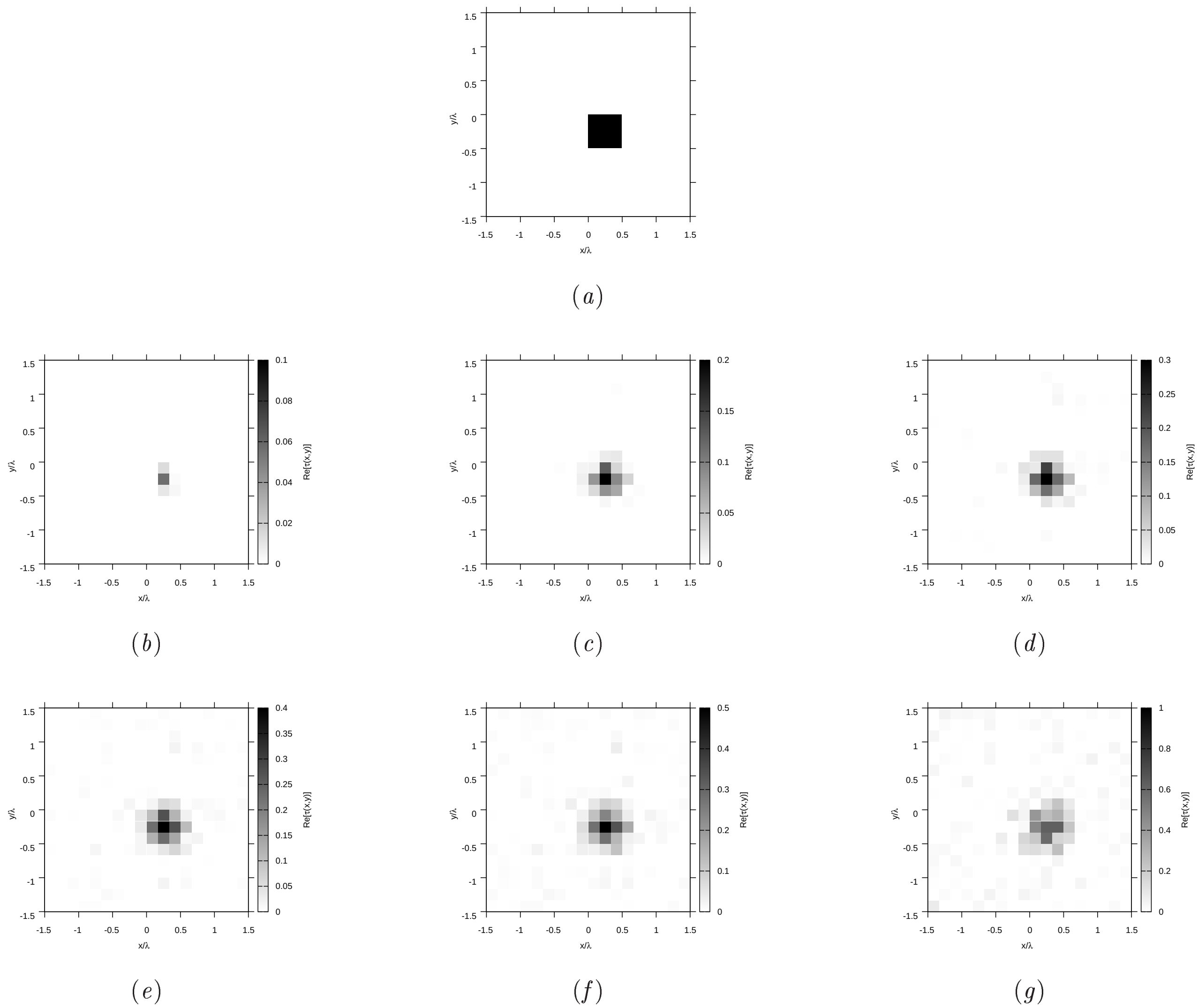

(a) (b) (c) (d) (e) (f) (g)

Figure 10. Actual object (a) and $(b)(c)(d)(e)(f)(g)$ BCS reconstructed object with (b) $\varepsilon_r = 1.1$, (c) $\varepsilon_r = 1.2$, (d) $\varepsilon_r = 1.3$, (e) $\varepsilon_r = 1.4$, (f) $\varepsilon_r = 1.5$ and (g) $\varepsilon_r = 2.0$.

RESULTS: Variable Square Cylinder Dimension - $L = \frac{2}{3}\lambda$

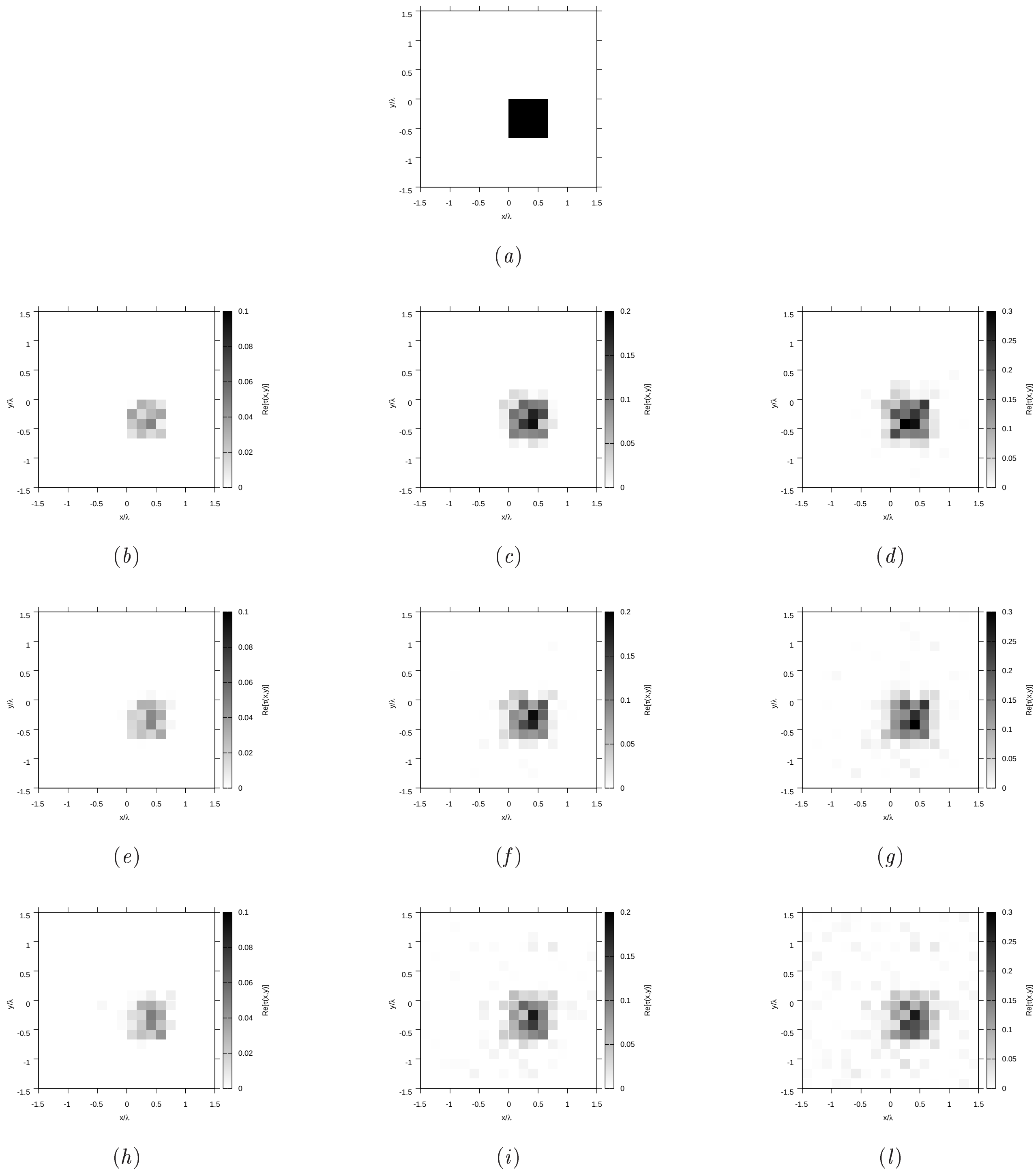

Figure 11. Actual object (a) and BCS reconstructed object with $(b)(e)(h)$ $\varepsilon_r = 1.1$, $(c)(f)(i)$ $\varepsilon_r = 1.2$, and $(d)(g)(l)$ $\varepsilon_r = 1.3$, for $(b)(c)(d)$ Noiseless case, $(e)(f)(g)$ $SNR = 10$ [dB] and $(h)(i)(l)$ $SNR = 5$ [dB].

RESULTS: Variable Square Cylinder Dimension - $L = \frac{5}{6}\lambda$

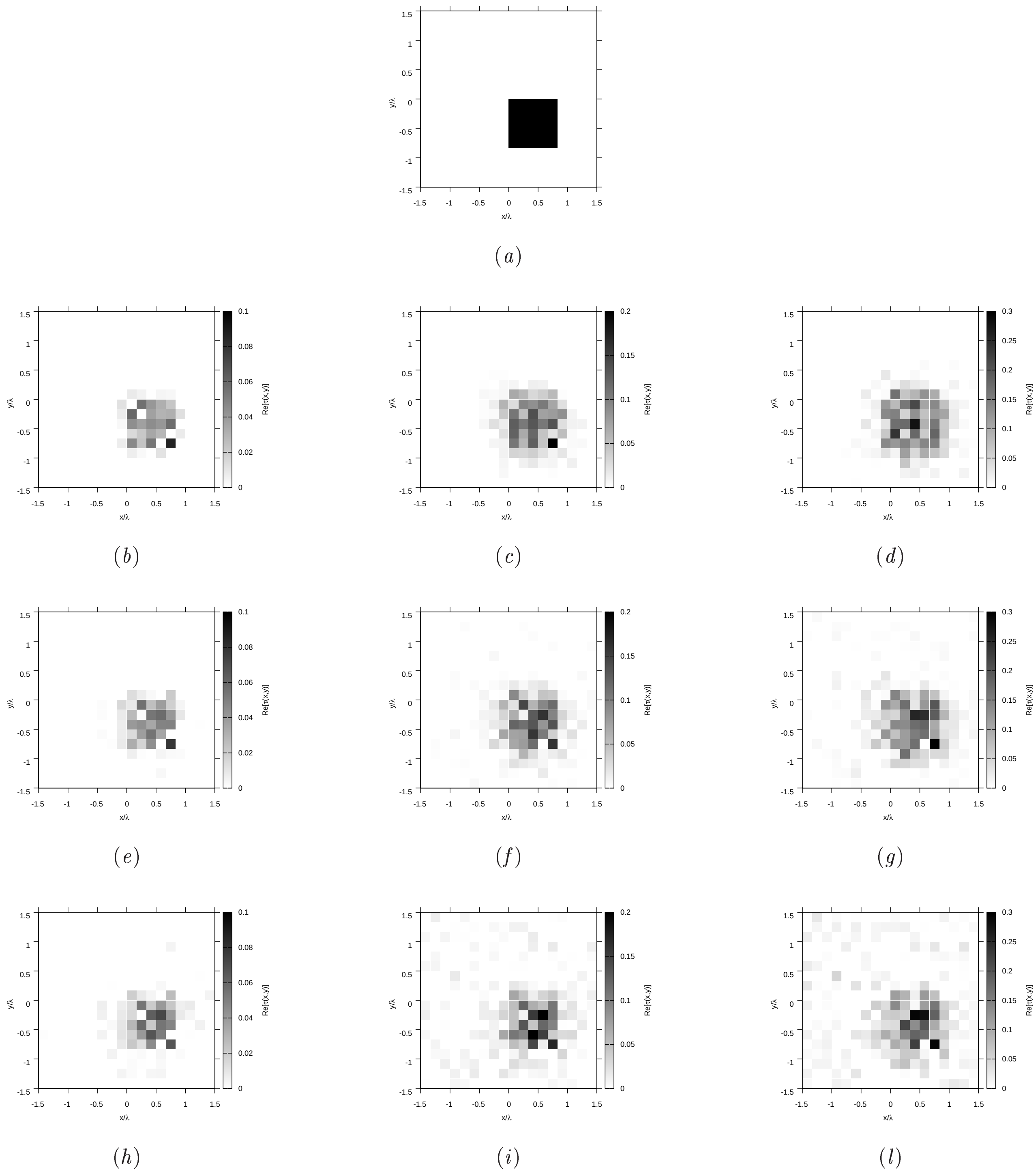

Figure 12. Actual object (a) and BCS reconstructed object with $(b)(e)(h)$ $\varepsilon_r = 1.1$, $(c)(f)(i)$ $\varepsilon_r = 1.2$, and $(d)(g)(l)$ $\varepsilon_r = 1.3$, for $(b)(c)(d)$ Noiseless case, $(e)(f)(g)$ $SNR = 10$ [dB] and $(h)(i)(l)$ $SNR = 5$ [dB].

RESULTS: Variable Square Cylinder Dimension - $L = \frac{\lambda}{6}$

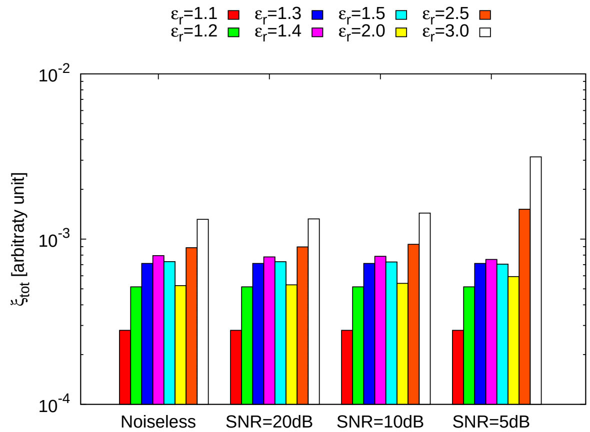

(a)

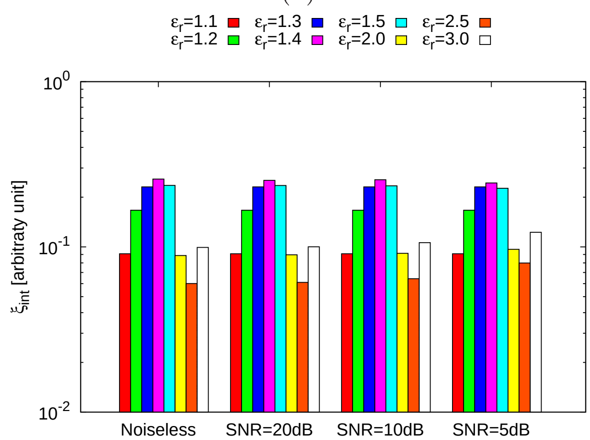

(b)

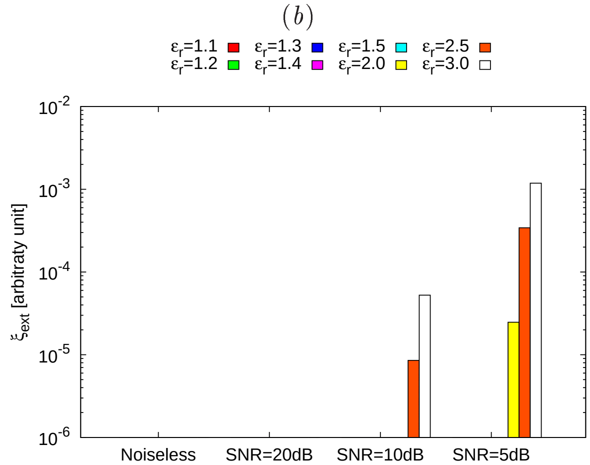

(c)

Figure 13. Behaviour of error figures for different ε_r and SNR values: (a) total error ξ_{tot}, (b) internal error ξ_{int}, (c) external error ξ_{ext}.

RESULTS: Variable Square Cylinder Dimension - $L = \frac{\lambda}{3}$

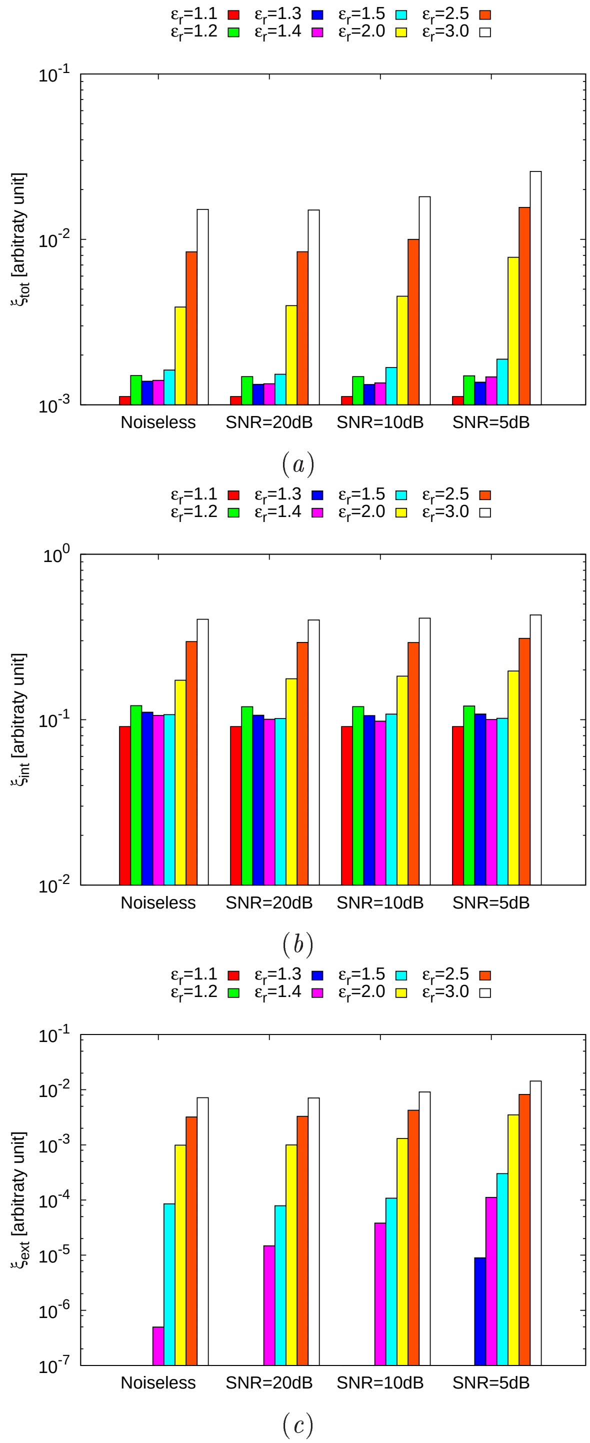

Figure 14. Behaviour of error figures for different ε_r and SNR values: (a) total error ξ_{tot}, (b) internal error ξ_{int}, (c) external error ξ_{ext}.

RESULTS: Variable Square Cylinder Dimension - $L = \frac{\lambda}{2}$

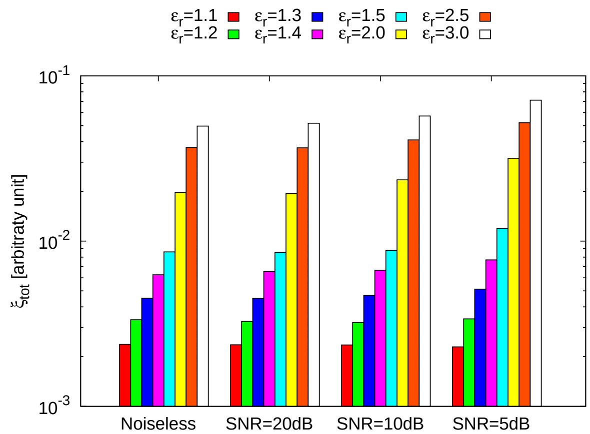

(a)

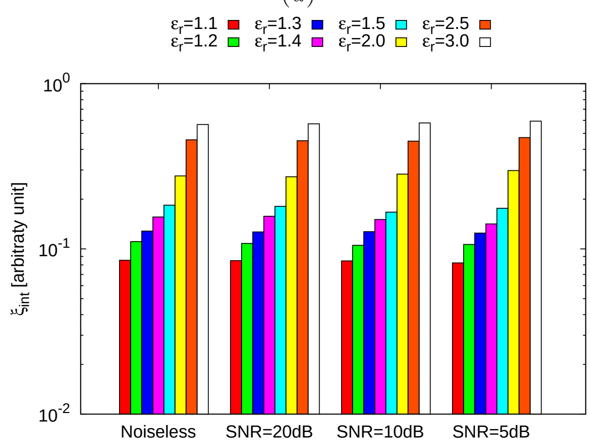

(b)

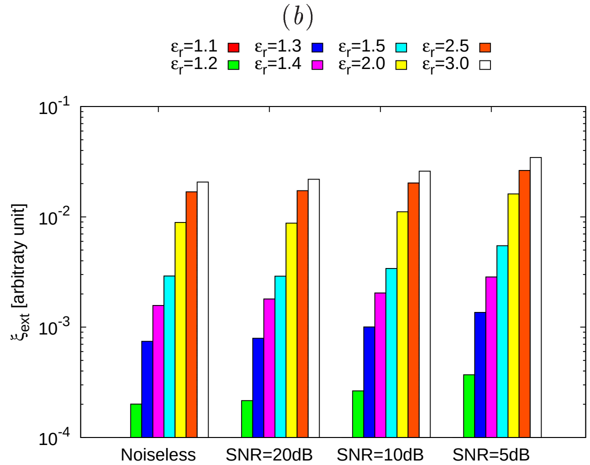

(c)

Figure 15. Behaviour of error figures for different ε_r and SNR values: (a) total error ξ_{tot}, (b) internal error ξ_{int}, (c) external error ξ_{ext}.

RESULTS: Variable Square Cylinder Dimension - $L = \frac{2}{3}\lambda$

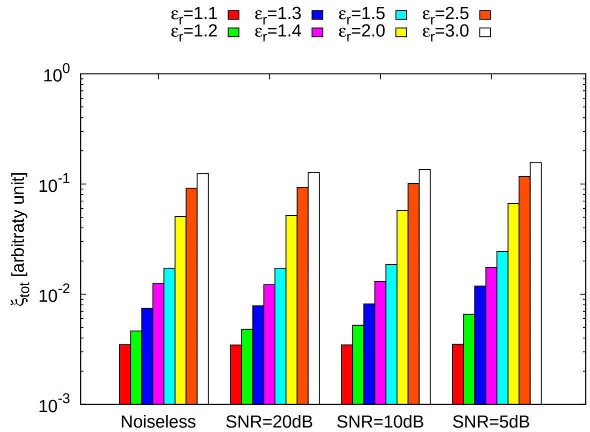

(a)

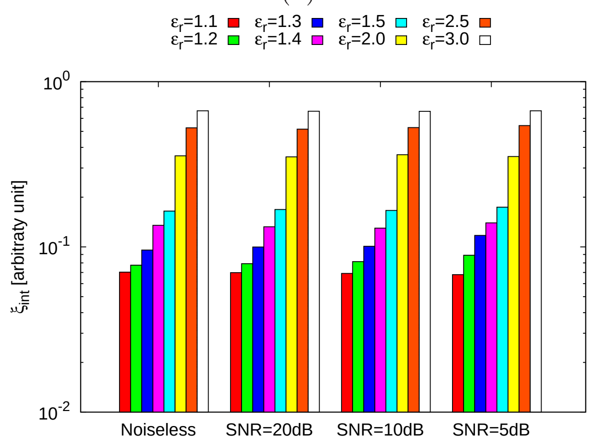

(b)

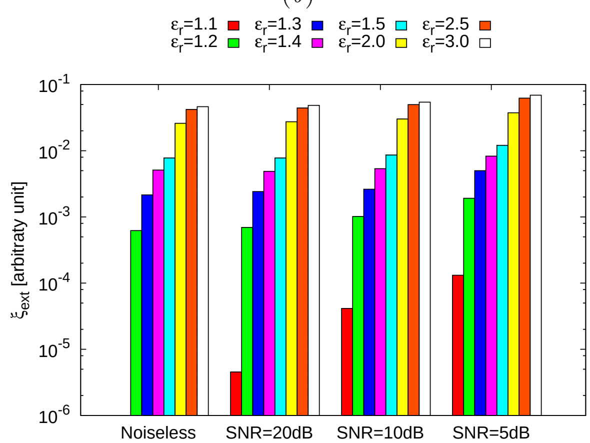

(c)

Figure 16. Behaviour of error figures for different ε_r and SNR values: (a) total error ξ_{tot}, (b) internal error ξ_{int}, (c) external error ξ_{ext}.

RESULTS: Variable Square Cylinder Dimension - $L = \frac{5}{6}\lambda$

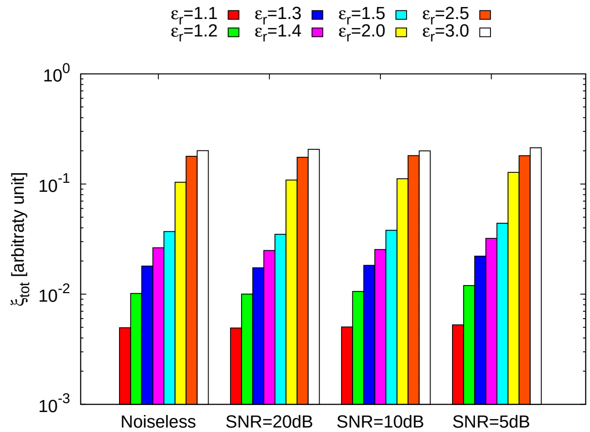

(a)

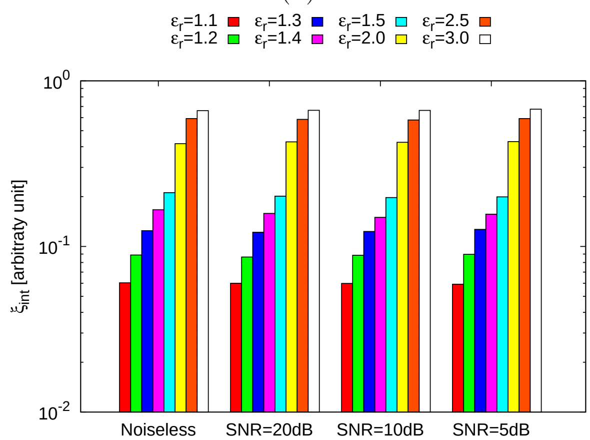

(b)

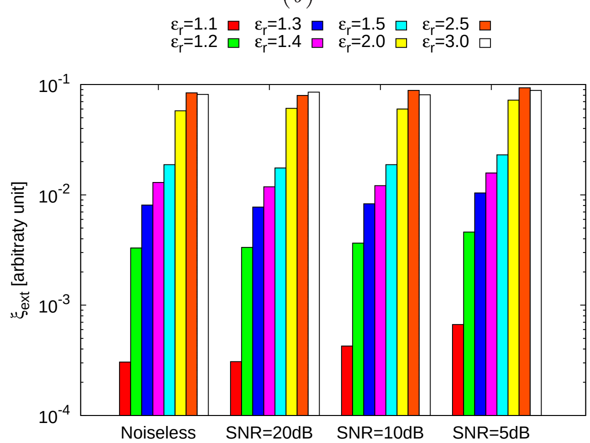

(c)

Figure 17. Behaviour of error figures for different ε_r and SNR values: (a) total error ξ_{tot}, (b) internal error ξ_{int}, (c) external error ξ_{ext}.

RESULTS: Variable Square Cylinder Dimension - $L = \lambda$

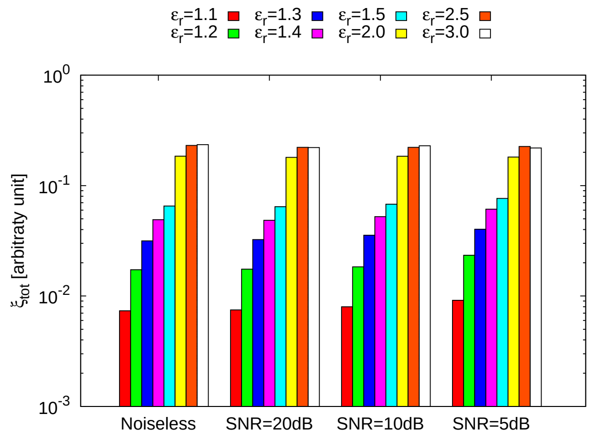

(a)

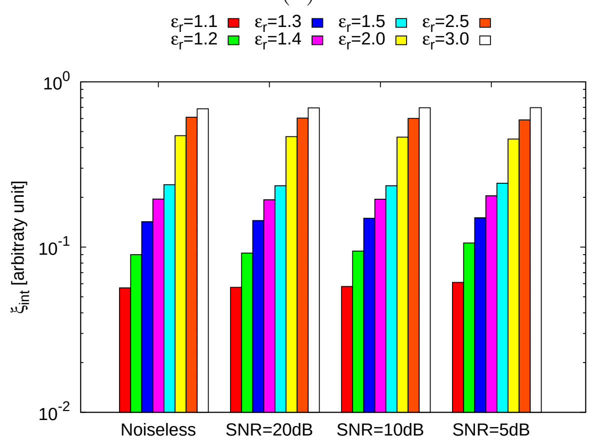

(b)

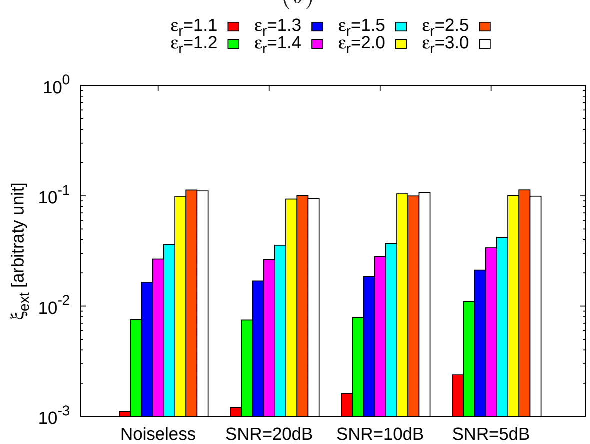

(c)

Figure 18. Behaviour of error figures for different ε_r and SNR values: (a) total error ξ_{tot}, (b) internal error ξ_{int}, (c) external error ξ_{ext}.

RESULTS: Variable Square Cylinder Dimension - Total Error ξ_{tot} - Comparison Born/Rytov Approximation

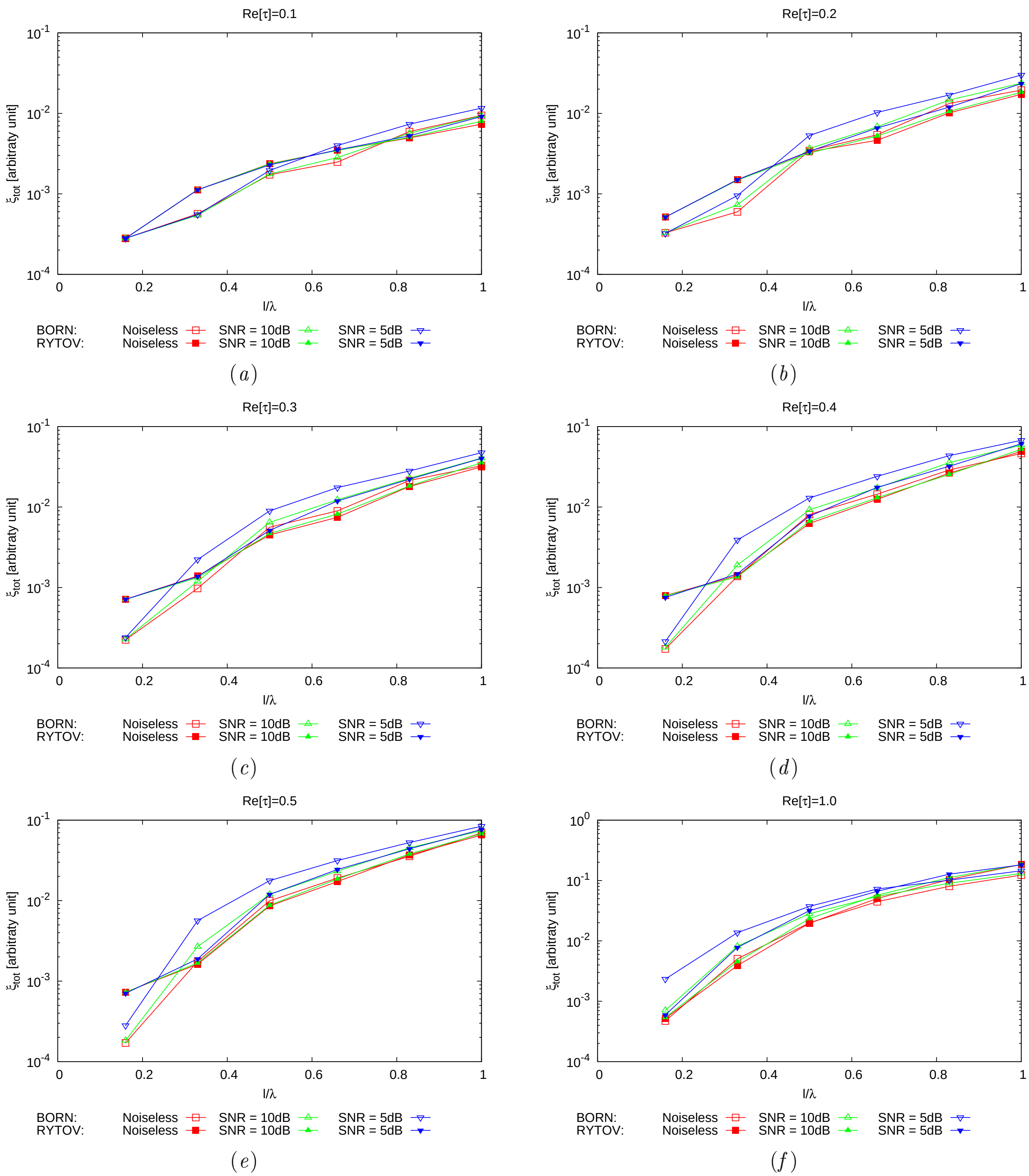

Figure 36. Behaviour of total error ξ_{tot} as a function of L, for different ε_r values: (a) $\varepsilon_r = 1.1$, (b) $\varepsilon_r = 1.2$, (c) $\varepsilon_r = 1.3$, (d) $\varepsilon_r = 1.4$, (e) $\varepsilon_r = 1.5$ and (f) $\varepsilon_r = 2.0$.

RESULTS: Variable Square Cylinder Dimension - Internal Error ξ_{int} - Comparison Born/Rytov Approximation

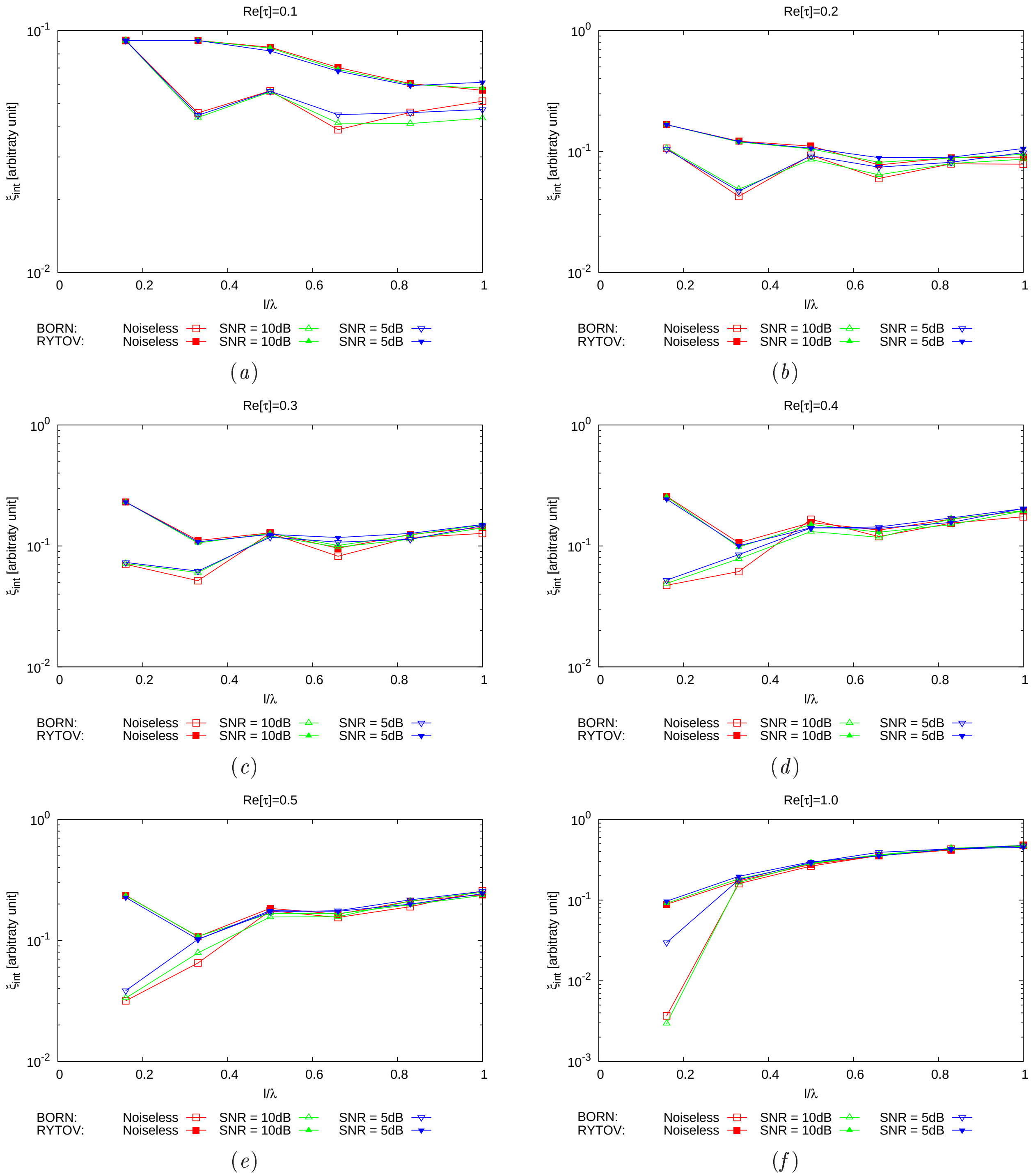

Figure 19. Behaviour of total error ξ_{tot} as a function of L, for different ε_r values: (a) $\varepsilon_r = 1.1$, (b) $\varepsilon_r = 1.2$, (c) $\varepsilon_r = 1.3$, (d) $\varepsilon_r = 1.4$, (e) $\varepsilon_r = 1.5$ and (f) $\varepsilon_r = 2.0$.

RESULTS: Variable Square Cylinder Dimension - External Error ξ_{ext} - Comparison Born/Rytov Approximation

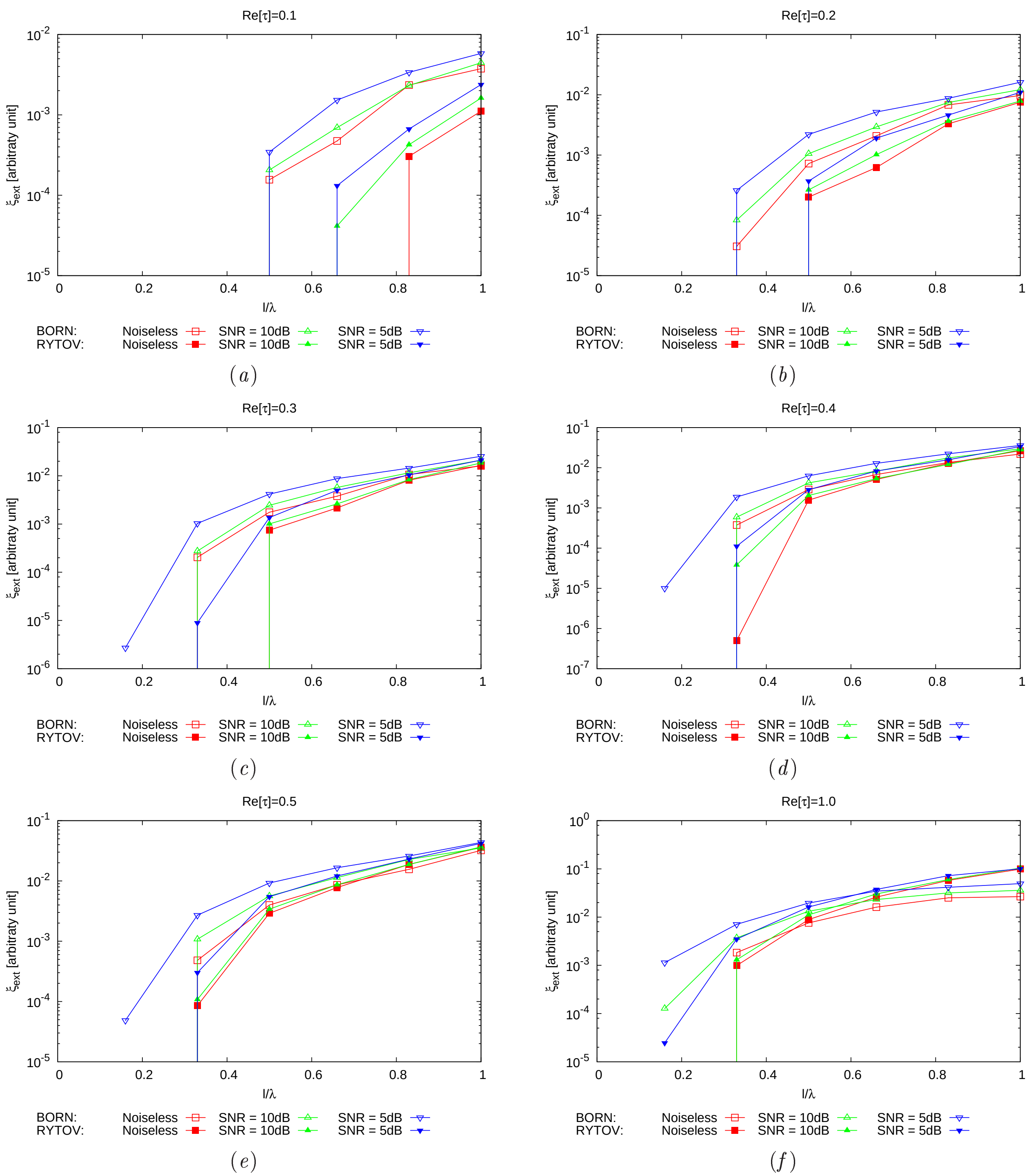

Figure 20. Behaviour of total error ξ_{tot} as a function of L, for different ε_r values: (a) $\varepsilon_r = 1.1$, (b) $\varepsilon_r = 1.2$, (c) $\varepsilon_r = 1.3$, (d) $\varepsilon_r = 1.4$, (e) $\varepsilon_r = 1.5$ and (f) $\varepsilon_r = 2.0$.

References

[1] L. Poli, G. Oliveri, and A. Massa, "Imaging sparse metallic cylinders through a Local Shape Function Bayesian Compressive Sensing approach," Journal of Optical Society of America A, vol. 30, no. 6, pp. 1261-1272, 2013.

[2] F. Viani, L. Poli, G. Oliveri, F. Robol, and A. Massa, "Sparse scatterers imaging through approximated multitask compressive sensing strategies," Microwave Opt. Technol. Lett., vol. 55, no. 7, pp. 1553-1558, Jul. 2013.

[3] L. Poli, G. Oliveri, P. Rocca, and A. Massa, "Bayesian compressive sensing approaches for the reconstruction of two-dimensional sparse scatterers under TE illumination," IEEE Trans. Geosci. Remote Sensing, vol. 51, no. 5, pp. 2920-2936, May. 2013.

[4] L. Poli, G. Oliveri, and A. Massa, "Microwave imaging within the first-order Born approximation by means of the contrast-field Bayesian compressive sensing," IEEE Trans. Antennas Propag., vol. 60, no. 6, pp. 2865-2879, Jun. 2012.

[5] G. Oliveri, P. Rocca, and A. Massa, "A bayesian compressive sampling-based inversion for imaging sparse scatterers," IEEE Trans. Geosci. Remote Sensing, vol. 49, no. 10, pp. 3993-4006, Oct. 2011.

[6] G. Oliveri, L. Poli, P. Rocca, and A. Massa, "Bayesian compressive optical imaging within the Rytov approximation," Optics Letters, vol. 37, no. 10, pp. 1760-1762, 2012.

[7] L. Poli, G. Oliveri, F. Viani, and A. Massa, "MT-BCS-based microwave imaging approach through minimum-norm current expansion," IEEE Trans. Antennas Propag., in press. doi:10.1109/TAP.2013.2265254

[8] G. Oliveri and A. Massa, "Bayesian compressive sampling for pattern synthesis with maximally sparse non-uniform linear arrays," IEEE Trans. Antennas Propag., vol. 59, no. 2, pp. 467-481, Feb. 2011.

[9] G. Oliveri, M. Carlin, and A. Massa, "Complex-weight sparse linear array synthesis by Bayesian Compressive Sampling," IEEE Trans. Antennas Propag., vol. 60, no. 5, pp. 2309-2326, May 2012.

[10] G. Oliveri, P. Rocca, and A. Massa, "Reliable Diagnosis of Large Linear Arrays - A Bayesian Compressive Sensing Approach," IEEE Trans. Antennas Propag., vol. 60, no. 10, pp. 4627-4636, Oct. 2012.

[11] F. Viani, G. Oliveri, and A. Massa, "Compressive sensing pattern matching techniques for synthesizing planar sparse arrays" IEEE Trans. Antennas Propag., in press. doi:10.1109/TAP.2013.2267195

[12] M. Carlin, P. Rocca, G. Oliveri, F. Viani, and A. Massa, "Directions-of-Arrival Estimation through Bayesian Compressive Sensing strategies," IEEE Trans. Antennas Propag., in press.

[13] M. Carlin, P. Rocca, "A Bayesian compressive sensing strategy for direction-of-arrival estimation," 6th European Conference on Antennas Propag. (EuCAP 2012), Prague, Czech Republic, pp. 1508-1509, 26-30 Mar. 2012.

[14] M. Carlin, P. Rocca, G. Oliveri, and A. Massa, "Bayesian compressive sensing as applied to directions-of-arrival estimation in planar arraysâ" Journal of Electrical and Computer Engineering, Special Issue on "Advances in Radar Technologiesâ" in press.

[15] M. Donelli, D. Franceschini, P. Rocca, and A. Massa, "Three-dimensional microwave imaging problems solved through an efficient multi-scaling particle swarm optimization," IEEE Trans. Geosci. Remote Sensing, vol. 47, no. 5, pp. 1467-1481, May 2009.

[16] M. Benedetti, G. Franceschini, R. Azaro, and A. Massa, "A numerical assessment of the reconstruction effectiveness of the integrated GA-based multicrack strategy," IEEE Antennas Wireless Propag. Lett., vol. 6, pp. 271-274, 2007.

[17] P. Rocca, M. Carlin, G. Oliveri, and A. Massa, "Interval analysis as applied to inverse scattering," IEEE International Symposium on Antennas Propag. (APS/URSI 2013), Chicago, Illinois, USA, Jul. 8-14, 2012.

[18] L. Manica, P. Rocca, M. Salucci, M. Carlin, and A. Massa, "Scattering data inversion through interval analysis under Rytov approximation," 7th European Conference on Antennas Propag. (EuCAP 2013), Gothenburg, Sweden, Apr. 8-12, 2013.

[19] P. Rocca, M. Carlin, and A. Massa, "Imaging weak scatterers by means of an innovative inverse scattering technique based on the interval analysis," 6th European Conference on Antennas Propag. (EuCAP 2012), Prague, Czech Republic, Mar. 26-30, 2012.

[20] S. C. Hagness, E. C. Fear, and A. Massa, "Guest Editorial: Special Cluster on Microwave Medical Imaging", IEEE Antennas Wireless Propag. Lett., vol. 11, pp. 1592-1597, 2012.

[21] G. Oliveri, Y. Zhong, X. Chen, and A. Massa, "Multi-resolution subspace-based optimization method for inverse scattering," Journal of Optical Society of America A, vol. 28, no. 10, pp. 2057-2069, Oct. 2011.

[22] A. Randazzo, G. Oliveri, A. Massa, and M. Pastorino, "Electromagnetic inversion with the multiscaling inexact-Newton method - Experimental validation," Microwave Opt. Technol. Lett., vol. 53, no. 12, pp. 2834-2838, Dec. 2011.

[23] G. Oliveri, L. Lizzi, M. Pastorino, and A. Massa, "A nested multi-scaling inexact-Newton iterative approach for microwave imaging," IEEE Trans. Antennas Propag., vol. 60, no. 2, pp. 971-983, Feb. 2012.

[24] G. Oliveri, A. Randazzo, M. Pastorino, and A. Massa, "Electromagnetic imaging within the contrast-source formulation by means of the multiscaling inexact Newton method," Journal of Optical Society of America A, vol. 29, no. 6, pp. 945-958, 2012.

[25] M. Benedetti, D. Lesselier, M. Lambert, and A. Massa, "Multiple shapes reconstruction by means of multi-region level sets," IEEE Trans. Geosci. Remote Sensing, vol. 48, no. 5, pp. 2330-2342, May 2010.

[26] M. Benedetti, D. Lesselier, M. Lambert, and A. Massa, "A multi-resolution technique based on shape optimization for the reconstruction of homogeneous dielectric objects," Inverse Problems, vol. 25, no. 1, pp. 1-26, Jan. 2009.